

Evolution of Hard X-Ray Radiation from Clusters of Galaxies: Bremsstrahlung or Inverse Compton Scattering?

Motokazu TAKIZAWA

Department of Physics, Yamagata University, Kojirakawa-machi 1-4-12, Yamagata 990-8560

takizawa@sci.kj.yamagata-u.ac.jp

Department of Astronomy, University of Virginia, P.O. Box 3818, Charlottesville, VA 22903-0818, USA

(Received ; accepted)

Abstract

We have calculated evolution of a non-thermal electron population from super-thermal but weakly relativistic to highly relativistic energy range in clusters of galaxies. We investigate evolution of hard X-ray radiation due to both bremsstrahlung and inverse Compton scattering of the cosmic microwave background photons. The bremsstrahlung component is more significant than the inverse Compton scattering one when the momentum spectra of electron sources are steeper than $\sim P_e^{-3.0}$ and vice versa in the case of Coma, where P_e is an electron momentum. The resultant hard X-ray spectra are flatter when the bremsstrahlung component is dominant. When the spectral indices of the source term are in the intermediate range ($-2.5 \sim -3.5$), too much extreme ultraviolet emission is produced. Inverse Compton dominant models can reproduce Coma cluster results with reasonable injection rates, which are possible in cluster mergers and/or ambient gas accretion.

Key words: galaxies: clusters: general — galaxies:clusters: individual (Coma) — intergalactic medium — radiation mechanisms: non-thermal

1. INTRODUCTION

Clusters of galaxies (CG) contain not only the thermal intracluster medium (ICM) but also non-thermal high energy particles in intracluster space. One of their direct evidences is existence of non-thermal synchrotron radio halos and relics, which have been observed since 1970s (Wilson 1970; Giovannini, Tordi, & Feretti 1999). This indicates that there are non-thermal electrons with energy of \sim GeV in intracluster space. Although their origin is still not clear, they are probably related with some active phenomena in CG such as cluster mergers, AGNs, AGNs' jets, and/or star burst in the member galaxies. Therefore, it is crucial to study non-thermal high energy particles in order to investigate active phenomena in CG. Furthermore, such non-thermal electrons and protons possibly have an effect on ICM dynamics (Rephaeli & Silk 1995; Inoue & Sasaki 2001) and Sunyaev-Zel'dovich effect (Blasi, Olinto, & Stebbins 2000; Ensslin & Kaiser 2000).

On the other hand, non-thermal hard X-ray radiation due to inverse Compton scattering (ICS) of cosmic microwave background (CMB) photons by the same electron population is expected from such CG with radio halos and relics (Rephaeli 1979). There have been many attempts to detect such high energy emission (e.g., Rephaeli, Ulmer, & Gruber 1994; Henriksen 1999; Valinia et al. 1999). However, because of the dominant thermal X-ray emission from ICM, it was very difficult to detect non-thermal hard X-ray radiation.

Recently, excess of hard X-ray radiation over thermal emission is detected from Coma (Fusco-Femiano et al. 1999; Rephaeli, Gruber, & Blanco 1999), A2256 (Fusco-Femiano et al. 2000), and HCG62 (Fukazawa et al. 2001) though their origin is still unclear. If we assume all hard X-ray radiation is due to ICS of CMB, we can estimate intracluster magnetic field strength or its lower limit by comparing hard X-ray flux or its upper limit with synchrotron radio flux, respectively (e.g., Fusco-Femiano et al. 1999; Henriksen 1999; Valinia et al. 1999). However, the magnetic field strength estimated through this method tends to be weaker than that determined through Faraday rotation measurement (Kim, Tribble & Kronberg 1991; Clarke, Kronberg, & Böhringer 2001).

One possible solution of this discrepancy is that all or a significant part of hard X-ray emission is due to non-thermal bremsstrahlung (NTB) from weakly relativistic non-thermal electrons with energy of a few 10 or 100 keV (e.g., Kaastra et al. 1999; Ensslin, Lieu, & Biermann 1999; Kempner & Sarazin 2000; Dogiel 2000; Blasi 2000). However, NTB needs much more non-thermal electron energy than ICS to produce a given amount of hard X-ray. In addition, dominant cooling process of electrons relevant to NTB hard X-ray is not bremsstrahlung losses but Coulomb interaction with thermal ICM, which results in energy transfer from the non-thermal electrons to the thermal ICM. Petrosian (2001) showed that unusual rapid heating will occur if Coma hard X-ray is due to NTB. However, calculation of NTB spectra is still interesting because it will possibly work well to explain future observations of other clusters. At present, hard

X-ray excess have been detected from only a few clusters of galaxies. Thus, it is not clear whether Coma cluster is a typical case or not.

Whether ICS or NTB is dominant in hard X-ray depends on a shape of electron momentum spectra. This depends on acceleration and cooling processes of electrons. For instance, if turbulent acceleration in ICM is an only effective acceleration process, it is difficult to accelerate thermal electrons up to \sim GeV because the acceleration time is too long for typical intracluster conditions. Therefore, almost hard X-ray is due to NTB (Blasi 2000). On the other hand, if we consider shock acceleration in ICM (Takizawa & Naito 2000), it is expected that accelerated electron momentum spectra are power-law up to the critical energy where an acceleration timescale is comparable to an ICS cooling timescale. For typical rich clusters, this critical energy is a few TeV (Loeb & Waxman 2000; Totani & Kitayama 2000). Thus, both ICS and NTB can contribute to hard X-ray radiation. When electron momentum spectra are single power-law, Sarazin and Kempner (2000) shows that NTB is dominant in hard X-ray if the momentum spectral index is more than ~ 2.7 .

Although accelerated electron momentum spectra in shocks are single power-law, total spectra in CG do not have to have the same form because various cooling processes can change the spectral shape. In a higher energy range, ICS and synchrotron loss modify the spectral shape from that of the source. In lower energy range, on the other hand, Coulomb loss does. Therefore, we have to follow time evolution of electron momentum spectra to investigate hard X-ray emission from CG.

In this paper, we calculate time evolution of electron momentum spectra for spherically symmetric models of CG and investigate evolution of both NTB and ICS contributions in hard X-ray. It is certain that the synchrotron radio spectrum of Coma is known to a much higher precision than its hard X-ray spectrum. However, synchrotron emissivity is proportional to the non-thermal electron density and the magnetic field energy density. Unfortunately, we do not have enough information about their spatial distribution. On the other hand, ICS and NTB emissivity are proportional to the non-thermal electron density and, the CMB energy density and the thermal ICM density, respectively. We have enough spatial information about both of them from radio and X-ray observations. Thus, we think calculating the NTB and ICS hard X-ray spectra is as useful as calculating synchrotron radio ones in order to consider physical property of non-thermal electrons in clusters of galaxies. The rest of this paper is organized as follows. In §2 we describe our models. In §3 we present the results. In §4 we compare our models to Coma cluster and discuss their implications. Finally, our conclusions are presented in §5.

2. MODELS

2.1. Evolution of Electron Momentum Spectra

To follow evolution of momentum spectra of a non-thermal electron population, we should solve a diffusion loss equation (Sarazin 1999). According to Bohm diffusion approximation, however, the spatial diffusion term is negligible in typical intracluster conditions within a few Gyrs (Takizawa & Naito 2000). We consider an isotropic momentum distribution function. It is not clear whether the electron pitch angle distribution is randomized or not in typical intracluster conditions. However, this isotropic assumption is clearly valid when we consider Inverse Compton, bremsstrahlung, and Coulomb losses because Faraday rotation measurements toward clusters of galaxies suggest tangled magnetic field in intracluster space. Chaotic field lines also give rise to isotropic emission independent of the electron pitch angle distribution. Only synchrotron loss rate depends on the pitch angle distribution but it does not dominate other loss processes within our parameter range. We consider spherically symmetric ICM for simplicity. We will use the normalized electron momentum defined by $p_e \equiv P_e/(m_e c)$. Let $N(p_e, r, t)dp_e$ be the number density of non-thermal electrons with momenta from p_e to $p_e + dp_e$ at the radius r . Thus, the equation which describes time evolution of $N(p_e, r, t)$ is,

$$\frac{\partial N(p_e, r, t)}{\partial t} = \frac{\partial}{\partial p_e} [b(p_e, r)N(p_e, r, t)] + Q(p_e, r, t), \quad (1)$$

where, $b(p_e, r)$ is the rate of normalized momentum loss for a single electron with a normalized momentum of p_e at the radius r , and $Q(p_e, r, t)$ gives the rate of production of new non-thermal electrons.

We consider ICS of the CMB photons, synchrotron loss, and Coulomb loss to determine $b(p_e, r)$. Bremsstrahlung loss is neglected because it does not contribute significantly in our parameter range. Thus,

$$b(p_e, r) = -\left(\frac{dp_e}{dt}\right)_{\text{IC}} - \left(\frac{dp_e}{dt}\right)_{\text{sync}} - \left(\frac{dp_e}{dt}\right)_{\text{Coul}}. \quad (2)$$

Each component is numerically (see Longair 1997),

$$-\left(\frac{dp_e}{dt}\right)_{\text{IC}} = 4.32 \times 10^{-4} \frac{p_e^2}{p_e^2 + 1} \rho_e^2 \text{Gyr}^{-1}, \quad (3)$$

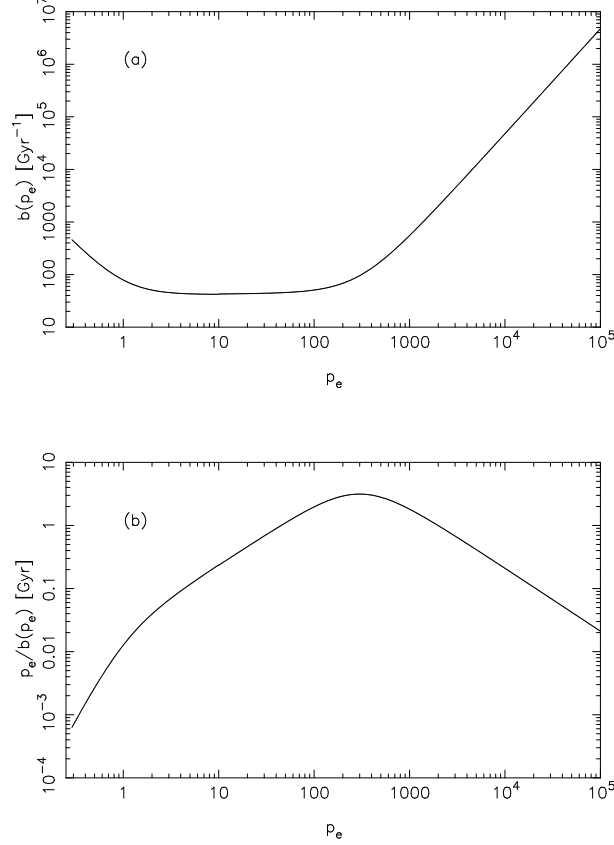


Fig. 1. (a) An electron momentum loss rate $b(p_e)$ as a function of p_e . (b) Electron cooling time defined by $p_e/b(p_e)$. In both cases we assume $n_e = 10^{-3} \text{cm}^{-3}$ and $B = 1 \mu\text{G}$. ICS loss is dominant for a higher energy region ($p_e \gg 100$), where $b(p_e) \propto p_e^2$ and $p_e/b(p_e) \propto p_e^{-1}$. The loss rate is well approximated by Coulomb loss with an extremely relativistic limit in a middle region ($p_e \sim 10$), where $b(p_e)$ is almost constant and $p_e/b(p_e) \propto p_e$. Transrelativistic effect appears in a lower energy part ($p_e \sim 1$), where $b(p_e) \propto (p_e^2 + 1)/p_e^2$ and $p_e/b(p_e) \propto p_e^3/(p_e^2 + 1)$ approximately.

$$-\left(\frac{dp_e}{dt}\right)_{\text{sync}} = 4.10 \times 10^{-5} \frac{p_e^2}{p_e^2 + 1} p_e^2 \left(\frac{B}{\mu\text{G}}\right)^2 \text{Gyr}^{-1}, \quad (4)$$

$$-\left(\frac{dp_e}{dt}\right)_{\text{Coul}} = 3.79 \times 10 \left(\frac{n_e}{10^{-3} \text{cm}^{-3}}\right) \frac{p_e^2 + 1}{p_e^2} \left(1.0 + \frac{\ln\left(\frac{p_e^2}{p_e^2 + 1}\right)}{19} + \frac{\ln\left(\frac{\sqrt{p_e^2 + 1}}{n_e/\text{cm}^{-3}}\right)}{75}\right) \text{Gyr}^{-1}, \quad (5)$$

where B is the intracluster magnetic field strength, and n_e is the electron density of thermal ICM. We consider CMB photons at $z=0$ as soft photon density calculating inverse Compton loss rate. We use 2.7 K as CMB temperature.

The loss rate $b(p_e)$ and cooling time defined by $p_e/b(p_e)$ are shown in Figure 1 as a function of p_e when $n_e = 10^{-3} \text{cm}^{-3}$ and $B = 1 \mu\text{G}$. ICS loss is dominant for a higher energy region ($p_e \gg 100$), where $b(p_e) \propto p_e^2$ and $p_e/b(p_e) \propto p_e^{-1}$. The loss rate is well approximated by Coulomb loss with an extremely relativistic limit in a middle region ($p_e \sim 10$), where $b(p_e)$ is almost constant and $p_e/b(p_e) \propto p_e$. Transrelativistic effect appears in a lower energy part ($p_e \sim 1$), where $b(p_e) \propto (p_e^2 + 1)/p_e^2$ and $p_e/b(p_e) \propto p_e^3/(p_e^2 + 1)$ approximately.

We assume that $Q(p_e, t) \propto p_e^{-\mu}$, which is expected from the standard theory of shock acceleration. We neglect the temporal change of the index μ .

2.2. Emission from a non-thermal electron population

Let $l_\epsilon(r)$ be the volume emissivity of non-thermal hard X-ray at energies from ϵ to $\epsilon + d\epsilon$ at the radius r . We consider NTB and ICS of CMB photons from a non-thermal electron population,

$$l_\epsilon(r) = l_\epsilon^{\text{NTB}}(r) + l_\epsilon^{\text{ICS}}(r). \quad (6)$$

For NTB components, the emission is given by the integral (see Sarazin & Kempner 2000),

$$l_\epsilon^{\text{NTB}}(r) = \epsilon \int N(p_1, r) dp_1 v(p_1) \sum_Z n_Z(r) \frac{d\sigma(p_1, \epsilon, Z)}{d\epsilon}, \quad (7)$$

where, $v(p_1) = cp_1/(p_1^2 + 1)^{1/2}$ is the velocity of an electron with normalized electron momentum p_1 , Z is the charge of the various thermal particles in ICM, $n_Z(r)$ is the number densities of these thermal particles at r , and $[d\sigma(p_1, \epsilon, Z)/d\epsilon]d\epsilon$ is the bremsstrahlung cross section for emitting photons with energies from ϵ to $\epsilon + d\epsilon$ for the collision between an electron with normalized momentum p_1 and an ion with electric charge Ze .

To calculate the cross sections, we use the Born-approximation formulas of completely unscreened nuclei (Koch & Motz 1959). We use the extreme-relativistic limit of Bethe-Heitler formula for the extremely relativistic ($p_e > 4.81$) electrons. On the other hand, we use the transrelativistic expressions of equations (2) and (4) in Haug (1997) for weakly relativistic electrons ($p_e < 0.965$) and moderately relativistic ($0.965 < p_e < 4.81$) electrons, respectively. The distortion of the electron wave function by the nuclear Coulomb field is considered by multiplying the Elwert factor.

For ICS components, the emission is (see Blumenthal & Gould 1970),

$$l_\epsilon^{\text{ICS}}(r) = \frac{12\pi\sigma_T}{h} \int N(\gamma, r) d\gamma \int_0^1 J\left(\frac{\epsilon}{4h\gamma^2 x}\right) F(x) dx, \quad (8)$$

where σ_T is the Thomson cross section, h is the Plank constant and

$$F(x) \equiv 1 + x + 2x \ln x - 2x^2. \quad (9)$$

$J(\nu)$ is the mean intensity at frequency ν of the seed photon field. For the CMB, this is the black body function

$$J(\nu) = \frac{2h\nu^3}{c^2} \frac{1}{\exp(h\nu/kT_{\text{CMB}}) - 1}. \quad (10)$$

The luminosity at energies from ϵ to $\epsilon + d\epsilon$ from a whole cluster L_ϵ is obtained by spatial integration of the above-mentioned volume emissivity,

$$L_\epsilon = L_\epsilon^{\text{NTB}} + L_\epsilon^{\text{ICS}}, \quad (11)$$

where,

$$L_\epsilon^{\text{NTB}} = \int l_\epsilon^{\text{NTB}} 4\pi r^2 dr, \quad (12)$$

$$L_\epsilon^{\text{ICS}} = \int l_\epsilon^{\text{ICS}} 4\pi r^2 dr. \quad (13)$$

2.3. Model Clusters

For the thermal ICM, we assume the isothermal beta model (Cavaliere&Fusco-Femiano 1978). The electron number density of ICM at the radius r is,

$$n_e(r) = n_{e,0} \left[1 + \left(\frac{r}{r_c} \right)^2 \right]^{-\frac{3}{2}\beta}, \quad (14)$$

and the temperature T is constant. In order to compare our results with Coma cluster in §4, the parameters of Coma are used. We set $n_0 = 3.12 \times 10^{-3} \text{cm}^{-3}$, $r_c = 0.386 \text{Mpc}$, and $\beta = 0.705$ (Mohr, Mathiesen & Evrard 1999) and $kT = 8.5 \text{keV}$ (Fusco-Femiano et al. 1999). We assume that $n_e(r) = 0.0$ at $r > 2 \text{Mpc}$. This outer boundary is roughly equal to that of the observed thermal X-ray emission. As a result, the total number of thermal electrons is 2.22×10^{43} and the total thermal energy of electrons is $4.52 \times 10^{63} \text{erg}$. We assume $B = 1 \mu\text{G}$. Evolution of non-thermal electrons hardly depends on the magnetic field strength unless magnetic field energy density becomes comparable to or more than CMB one.

For the non-thermal electron populations, we assume that constant injection for a fiducial period t_{inj} and that momentum dependence of the injection rate is power-law. We assume that this single power-law form spectrum is valid between $p_{e,\text{min}} < p_e < p_{e,\text{max}}$, where $p_{e,\text{min}}$ is taken to be the normalized momentum corresponding to $E_e = 3kT$ and $p_{e,\text{max}}$ is assumed to be 10^7 , which is comparable to the critical energy of typical rich clusters up to which shock accelerated electron momentum spectra are power-law (Loeb & Waxman 2000; Totani & Kitayama 2000). Thus, $Q(p_e, r, t)$ is,

$$Q(p_e, r, t) = \begin{cases} Q_0(r) p_e^{-\mu} & (0 \leq t \leq t_{\text{inj}}) \\ 0 & (t_{\text{inj}} < t), \end{cases} \quad (15)$$

where Q_0 has a dimension of number density per time. Some candidates are proposed for the origin of a non-thermal population. As for a electron component, however, shocks in ICM caused by cluster merger is believed to be the most promising because they have enough and more energy than other candidates such as AGNs or normal galaxies. Furthermore, it is difficult to explain the typical spatial size of radio halos and relics for point sources like AGNs and

galaxies because diffusion length within ICS cooling time is too short. In the present model, thus, we set $t_{\text{inj}} = 1\text{Gyr}$, which is roughly equal to the duration of shocks in cluster mergers (Takizawa 1999, 2000).

Spatial distribution of electron injection is not clear because it depends on detailed parameters of cluster mergers. Thus we set fairly simple assumption. We assume it is proportional to local electron thermal energy. Total local injected energy of the non-thermal population is assumed to be 5% of the total local energy of thermal electrons. Therefor, normalization of source term $Q_0(r)$ is,

$$Q_0(r) = 0.05 \times \left(\frac{n_e(r)}{t_{\text{inj}}} \right) \left(\frac{3kT}{2m_e c^2} \right) \left(\int_{p_{e,\text{min}}}^{p_{e,\text{max}}} p_e^{-\mu} (\sqrt{p_e^2 + 1} - 1) dp_e \right)^{-1}. \quad (16)$$

According to the standard theory of first-order Fermi acceleration, it is expected that exponents of momentum spectra μ are 2 in non-relativistic strong shocks (see Jones & Ellison 1991). However, fairly low Mach number shocks are expected in cluster mergers because the ICM of the pre-merger clusters is already hot (Takizawa 1999, 2000; Miniati et al. 2000). In fact, some X-ray observations support this idea (e.g., Markevitch, Sarazin & Vikhlinin 1999; Kikuchi et al. 2000). Thus we consider the cases of $\mu = 2.0, 2.5, 3.0, 3.5$, and 4.0

3. RESULTS

3.1. Evolution of Electron Momentum Spectra

Figure 2 shows evolution of a total electron momentum spectrum in the $\mu = 2.0$ model. In all models electron momentum spectra evolve in a similar way as follows. While fresh non-thermal electrons are provided ($0 < t < 1\text{Gyr}$), the spectra change from the original single power-law form ($\propto p_e^{-\mu}$) into a steady state solution where the injection balances with the cooling. In the higher energy range the spectra change from $N(p_e) \propto p_e^{-\mu}$ into $p_e^{-(\mu+1)}$ because ICS cooling is dominant. In the lower energy range, on the other hand, the spectra change into $N(p_e) \propto p_e^{-\mu+3}/(p_e^2 + 1)$ because Coulomb loss is dominant. After the injection stops ($t > 1\text{Gyr}$), inverse Compton cut-off appears and shifts towards lower energy as time proceeds. In the lower energy range, the spectra change into a steady state solution without a source term, $N(p_e) \propto p_e^2/(p_e^2 + 1)$.

3.2. Evolution of Hard X-ray radiation

Figure 3 shows evolution of hard X-ray (20-80 keV) band total luminosity. Solid lines indicate NTB components and dashed lines show ICS components. The flatter source electron spectra result in more ICS and less NTB emission. Both components are comparable to each other in hard X-ray when $\mu \simeq 3$. Sarazin & Kempner (2000) shows that both components are comparable to each other with $\mu \simeq 2.7$ when electron momentum spectra are single power-law. However, note that we consider different situations In our models, electron sources are power-law ($0 < t < 1\text{Gyr}$) or not active ($t > 1\text{Gyr}$) and evolution of electron spectra are fully calculated. In Sarazin & Kempner (2000), on the other hand, power-law electron spectra are assumed for "Power-law" models, which correspond to only a very early epoch ($t \sim 0$) in our models where cooling does not play a significant role. They also consider "Cooling Electrons" model, where spectra are assumed to be in a steady state without any sources. This corresponds to a phase where source is not active ($t > 1\text{Gyr}$) in our models. Our results are different than theirs because electron momentum spectra are much modified from a single power-law form in the source term because of the various cooling processes. In particular, spectral flattening in lower energy owing to Coulomb cooling is important.

Although total energy injected into a non-thermal electron population is the same value in all models, the flatter the source electron spectra are, the more luminous the total hard X-ray emission is. This is because the electrons related to ICS components lose their kinetic energy mainly through ICS loss while the electrons related to NTB components lose their kinetic energy mainly through not bremsstrahlung loss but Coulomb interaction with the thermal ICM. Thus, ICS dominant models are much more efficient for energy transformation from non-thermal electrons into hard X-ray radiation. This point is very important when the origin of non-thermal electrons is discussed.

After injection stops ($t > 1\text{Gyr}$), both components of hard X-ray emission decrease in all models. However, timescales of decline are rather different between NTB and ICS components. In all models ICS components decrease in the same way. The decline timescale of ICS components is determined by ICS cooling time of the relevant electrons, which is commonly \sim a Gyr for all models because energy of the related electrons is \sim GeV (see Fig. 1b). However, this is not the case for NTB components. The flatter the source spectra are, the more slowly NTB components decrease. The reason of this behavior is as follows. When the source spectra are flatter, equilibrium electron spectra are also flatter. Thus, not only weakly relativistic electrons but also higher energy (~ 100 MeV) electrons contribute to the hard X-ray through NTB significantly. While cooling time of weakly relativistic ($\sim 10 - 100$ keV) electrons is very short ($\sim 10^{6-7}$ yr, see Fig. 1b), that of ~ 100 MeV electrons is fairly long (\sim a few Gyr). As a result, the contribution from higher energy electrons survives for several Gyrs in NTB hard X-ray. This is more prominent when the source spectra are flatter.

Observed hard X-ray spectra are often parameterized by a single power-law model. Thus, we fit our resultant total

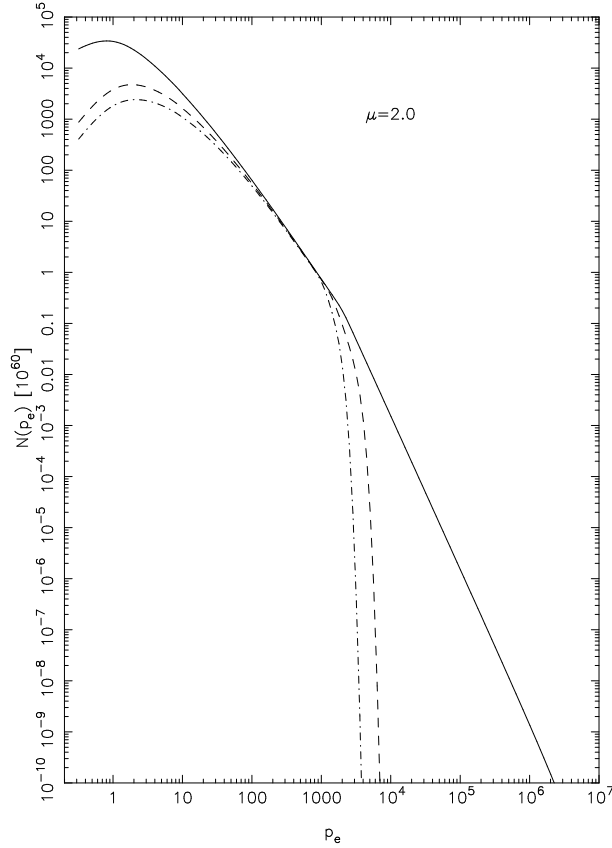


Fig. 2. Evolution of a total electron momentum spectrum in the $\mu = 2.0$ model. The different lines correspond to different epochs: $t = 1.0$ Gyr, solid line; $t = 1.5$ Gyr, dashed line; $t = 2.0$ Gyr, dot-dashed line. While fresh non-thermal electrons are provided ($0 < t < 1$ Gyr), the spectra change from the original single power-law form into a steady state solution. In the higher energy range the spectra change from $N(p_e) \propto p_e^{-2}$ into p_e^{-3} because of ICS cooling. In the lower energy range, the spectra change into $N(p_e) \propto p_e/(p_e^2 + 1)$ because of Coulomb loss. After the injection stops ($t > 1$ Gyr), inverse Compton cut-off appears and shifts towards lower energy as time proceeds. In the lower energy range, the spectra change into a steady state solution without a source term, $N(p_e) \propto p_e^2/(p_e^2 + 1)$.

hard X-ray spectra into a single power-law model ($L_\epsilon \propto \epsilon^\alpha$) to get a spectral index α . Figure 4 shows evolution of the spectral indices of total hard X-ray (20-80 keV) spectra. The behavior depends on whether ICS or NTB components are dominant. When ICS components are dominant ($\mu < 3.0$), spectral indices α changes from $-(\mu - 1)/2$ into $-\mu/2$ while the source is active ($0 < t < 1$ Gyr). After the injection stops, the indices become much smaller values because the inverse Compton cut-off enters a hard X-ray range. When NTB components are dominant ($\mu > 3.0$), on the other hand, the indices evolve in a rather different way. They become steady state values more quickly. In this stage, the indices are ~ -0.8 within our models. After the injection stops ($t > 1$ Gyr), they become ~ -0.15 , which is an approximation to a spectrum that varies as the logarithm of the photon energy (see Sarazin & Kempner 2000). In this way, NTB dominant models result in rather flat hard X-ray spectra.

NTB flux is proportional to a volume integral of the square of the ICM density because we assume that injection of non-thermal electrons is proportional to the local ICM density. On the other hand, ICS flux is proportional to a volume integral of the ICM density itself. As a result, this ratio is proportional to density weighted mean density of ICM $\langle n_e \rangle$ defined as follows,

$$\langle n_e \rangle \equiv \frac{\int n_e(r)^2 r^2 dr}{\int n_e(r) r^2 dr}. \quad (17)$$

X-ray observations shows that a core radius r_c is correlated with central density $n_{e,0}$. Fujita & Takahara (1999a, b) shows

$$\left(\frac{n_{e,0}}{\text{cm}^{-3}} \right) \simeq 6.4 \times 10^{-4} \left(\frac{r_c}{\text{Mpc}} \right)^{-1.3} \quad (18)$$

though a dispersion of a factor of three or four is seen in the data. Using this correlation, we plot $\langle n_e \rangle$ as a function of r_c in figure (5). Solid and dashed lines indicate cases of $\beta = 0.6$ and 0.7 , respectively. A square point shows the

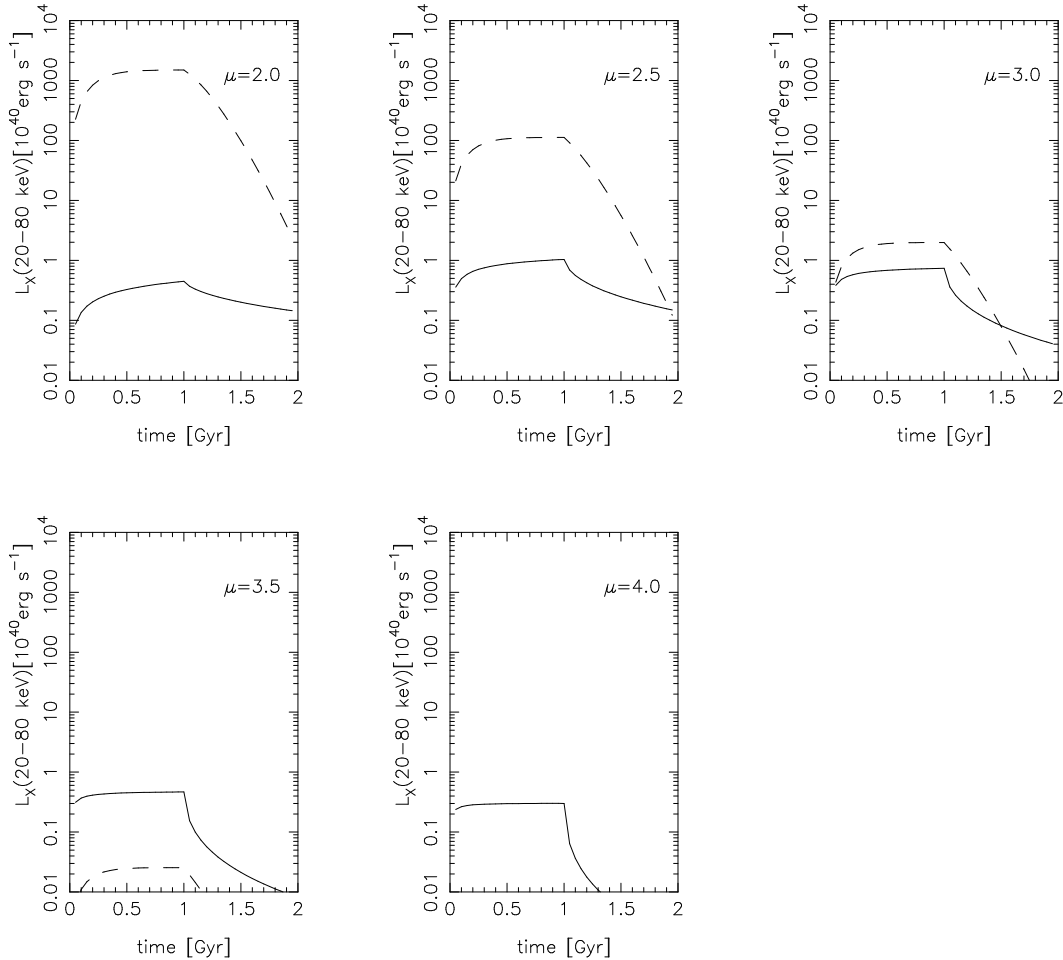


Fig. 3. Evolution of total hard X-ray (20-80 keV) luminosity of each model. Solid and dashed lines show bremsstrahlung and inverse Compton components, respectively. The flatter source electron spectra result in more ICS and less NTB emission. Both components are comparable to each other in hard X-ray when $\mu \simeq 3$.

Coma cluster. This figure shows $\langle n_e \rangle$ can become about twice of that of Coma in relatively high density clusters which follow the correlation. If we take a dispersion in the correlation into account, $\langle n_e \rangle$ can be nearly ten times larger than that of Coma. Therefore, the flux ratio of NTB to ICS can be about ten times higher than the values in figure 3 for relatively high density clusters.

4. COMPARISON WITH COMA CLUSTER

In this section, we compare our models with the Coma cluster. We compare a spectral shape of hard X-ray and a luminosity ratio of hard X-ray to EUV of our models with Coma. Then we seek an energy injection rate which can reproduce Coma for each model with different values of μ and discuss their implications. In Coma, a power-law model gives flux of 2.2×10^{-11} ergs cm^{-2} s^{-1} in the 20-80 keV band (Fusco-Femiano et al. 1999). This corresponds to luminosity of 5.1×10^{43} erg s^{-1} in the same band. The spectral index of hard X-ray from Coma is poorly determined. $0.3 \geq \alpha \geq -1.5$ is inferred at the 90% confidence level. In our parameter range of μ ($2.0 \leq \mu \leq 4.0$), thus, all models can reproduce this fact while fresh non-thermal electrons are provided (see a region of $0 \leq t \leq 1$ Gyr in Figure 4). However, it is difficult for ICS dominant models to reproduce the above-mentioned range of α after the injection stops (see a region of $t > 1$ Gyr in Figure 4).

Excess EUV radiation is also detected in Coma. The luminosity ratio of hard X-ray to EUV can be used to constrain our models. In Coma, the excess EUV radiation is significantly detected only within $r < 0.64$ Mpc and a power-law model gives EUV luminosity of 1.5×10^{42} erg s^{-1} in the 65-245 eV band (Bowyer, Breghöfer & Korpela 1999). This gives a luminosity ratio $L_{\text{HXR}}/L_{\text{EUV}} = 34$. We calculate EUV luminosity due to ICS within $r < 0.64$ Mpc for each model and compare the ratios with this value. Figure 6 shows evolution of $L_{\text{HXR}}/L_{\text{EUV}}$ for each model (solid lines). An observed value of Coma derived from Fusco-Femiano et al. (1999) and Bowyer et al. (1999) is shown by dashed

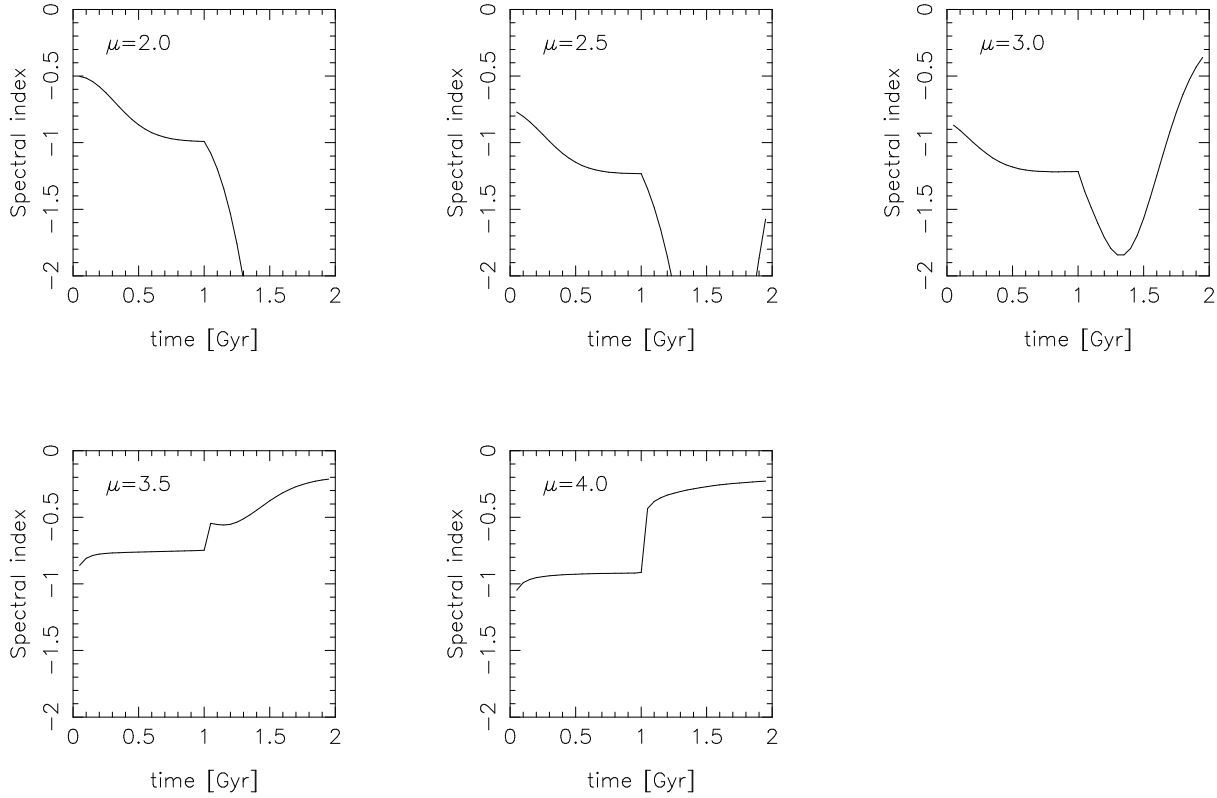


Fig. 4. Evolution of spectral indices in hard X-ray (20-80 keV) of each model. The behavior depends on whether ICS or NTB components are dominant. When ICS components are dominant ($\mu < 3.0$), spectral indices α changes from $-(\mu - 1)/2$ into $-\mu/2$ while the source is active ($0 < t < 1\text{Gyr}$). After the injection stops, the indices become much smaller values because the inverse Compton cut-off enters a hard X-ray range. When NTB components are dominant ($\mu > 3.0$), the indices are ~ -0.8 while sources are active. After the injection stops, they become ~ -0.15 .

lines. Note that $L_{\text{HXR}}/L_{\text{EUV}}$ of our models must be more than the observed value because ICS component from an old non-thermal electron population and/or thermal emission from warm gas possibly contribute to the observed EUV emission, which are not considered in our models. From figure 6 it is clear that this constraint is not satisfied when $\mu = 2.5$ and 3.0 . When $\mu = 3.5$, this can be satisfied only in a very early epoch ($t < 0.1$ Gyr). In other words, these models emit too much EUV compared with hard X-ray. On the other hand, models with $\mu = 2.0$ and 4.0 satisfy the above-mentioned constraint in an active phase ($0 < t < 1\text{Gyr}$). The reason is as follows. When ICS is dominant in hard X-ray ($\mu < 3$), the ratio of hard X-ray to EUV decreases as source spectra are steeper. This is because electrons relevant to hard X-ray have higher energy than those relevant to EUV. On the other hand, when NTB is dominant ($\mu > 3$), that ratio increases as source spectra are steeper because electrons relevant to hard X-ray have lower energy than those relevant to EUV. As a result, $\mu = 2.0$ and 4.0 models are favorable while $\mu = 2.5, 3.0$, and 3.5 models are not.

Although both ICS and NTB dominant models can be consistent with the observed hard X-ray spectral index of Coma, our NTB dominant models do not produce observed radio spectrum. For example, Deiss et al. (1997) shows the radio spectral index in the frequencies lower than 1.4 GHz is -1.16 , which means $\mu = 2.32$ in the electron source in an steady state. Therefore, another non-thermal electron component with flatter spectrum is necessary even if NTB is dominant in hard X-ray.

Next, we seek a numerical value of a total injected energy rate \dot{E}_{nth} which reproduce the Coma cluster hard X-ray luminosity at $t = 1$ Gyr. This is consistent with ICM temperature distribution derived from X-ray observation (Watanabe et al. 1999) and some numerical calculations of cluster merger (Burns et al. 1994; Ishizaka & Mineshige 1996) which suggest that Coma cluster is in major merger which started $\sim 0.5 - 1$ Gyr ago. Note that \dot{E}_{nth} is not very sensitive to accurate determination of an observational epoch because hard X-ray luminosity is nearly constant in all our models in $0.5\text{Gyr} < t < 1\text{Gyr}$. Then, we calculate total injected energy to the non-thermal population in 1 Gyr, $E_{\text{tot,nth}}$, and its ratio to the total electron thermal energy, $E_{\text{tot,nth}}/E_{\text{th}}$. The results for each model are shown in table 1.

From table 1, we find that NTB dominant models require very high rates of energy injection to explain the results of Coma cluster. This causes violent heating of thermal ICM unless duration of the acceleration process is very short

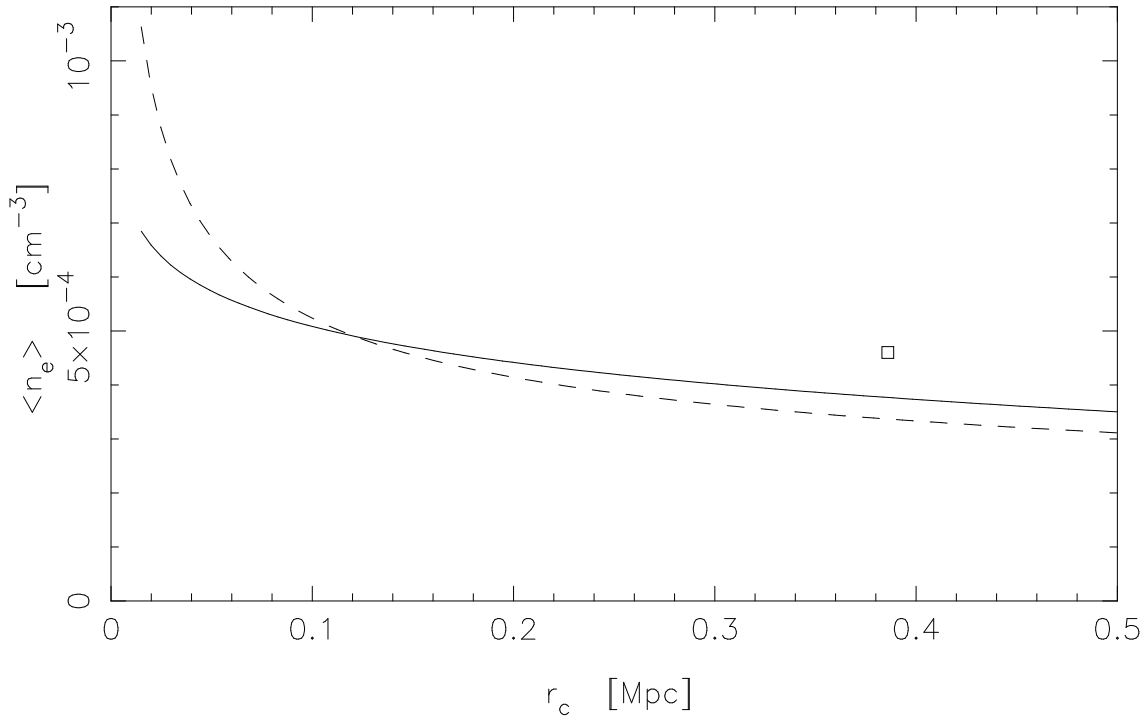


Fig. 5. Density-weighted mean density $\langle n_e \rangle$ as a function of r_c when we consider a correlation between r_c and $n_{e,0}$. Solid and dashed lines indicate cases of $\beta = 0.6$ and 0.7 , respectively. A square point shows a value of Coma cluster. $\langle n_e \rangle$ can become about twice of that of Coma in relatively high density clusters which follow the correlation. If we take a dispersion in the correlation into account, $\langle n_e \rangle$ can be nearly ten times larger than that of Coma.

(Petrosian 2001). Thus, we conclude that it is very difficult to consider NTB components significantly contribute to hard X-ray emission of Coma.

On the other hand, ICS dominant models are free from the difficulties mentioned above. The required injection rate is $\sim 10^{46-47} \text{ erg s}^{-1}$. This value can be realized by cluster mergers. Thus, ICS components are more likely as an origin of Coma hard X-ray in point of required energy. As many authors pointed, however, the flux ratio of synchrotron radio to hard X-ray gives us the volume averaged magnetic field strength in this case, which must coincide with that determined from Faraday rotation toward individual polarized radio galaxies unless spatial inhomogeneity plays a significant role. (e.g., Fusco-Femiano et al. 1999; Ensslin, Lieu, & Biermann 1999; Kempner & Sarazin 2000). We should look for any other causes of this discrepancy. For example, we should consider the spatial structure of magnetic field, inhomogeneity of magnetic field and non-thermal electrons, or spatial anti-correlation of magnetic field strength and non-thermal electron density, etc. Selection bias and Galactic contamination are extensively discussed by Goldshmidt & Rephaeli (1993) as the possible origin of this discrepancy.

5. CONCLUSIONS

We calculate evolution of a non-thermal electron population in clusters of galaxies and investigate hard X-ray radiation due to both NTB and ICS. We calculate cases where the electron sources are power-low in momentum ($\propto p_e^{-\mu}$). With the parameters of Coma, ICS components dominate NTB ones in hard X-ray radiation when $\mu < 3.0$ and vice versa. This dividing line may depend on thermal ICM density distribution. NTB dominant models have fairly flat hard X-ray spectra.

We compare our models to the Coma cluster. Luminosity ratio of hard X-ray to EUV is consistent with Coma when $\mu = 2.0$ and 4.0 . When $\mu = 3.5$, it is consistent only in a very early epoch. However, NTB dominant models require very high energy injection rates and cause unusual violent heating of thermal ICM unless duration of injection is very short (Petrosian 2001). On the other hand, ICS dominant models require much lower injection rates, which can be realized by cluster mergers. Thus, we conclude that ICS is more likely as the origin of Coma hard X-ray. In this case, however, the flux ratio of synchrotron radio to ICS hard X-ray gives us the volume averaged magnetic field strength. This value must coincide with that determined from Faraday rotation toward individual polarized radio galaxies unless spatial inhomogeneity plays a significant role. Thus, we should look for other solutions for the apparent discrepancy between magnetic field strength derived from the above-mentioned two methods. It may be related to spatial configurations

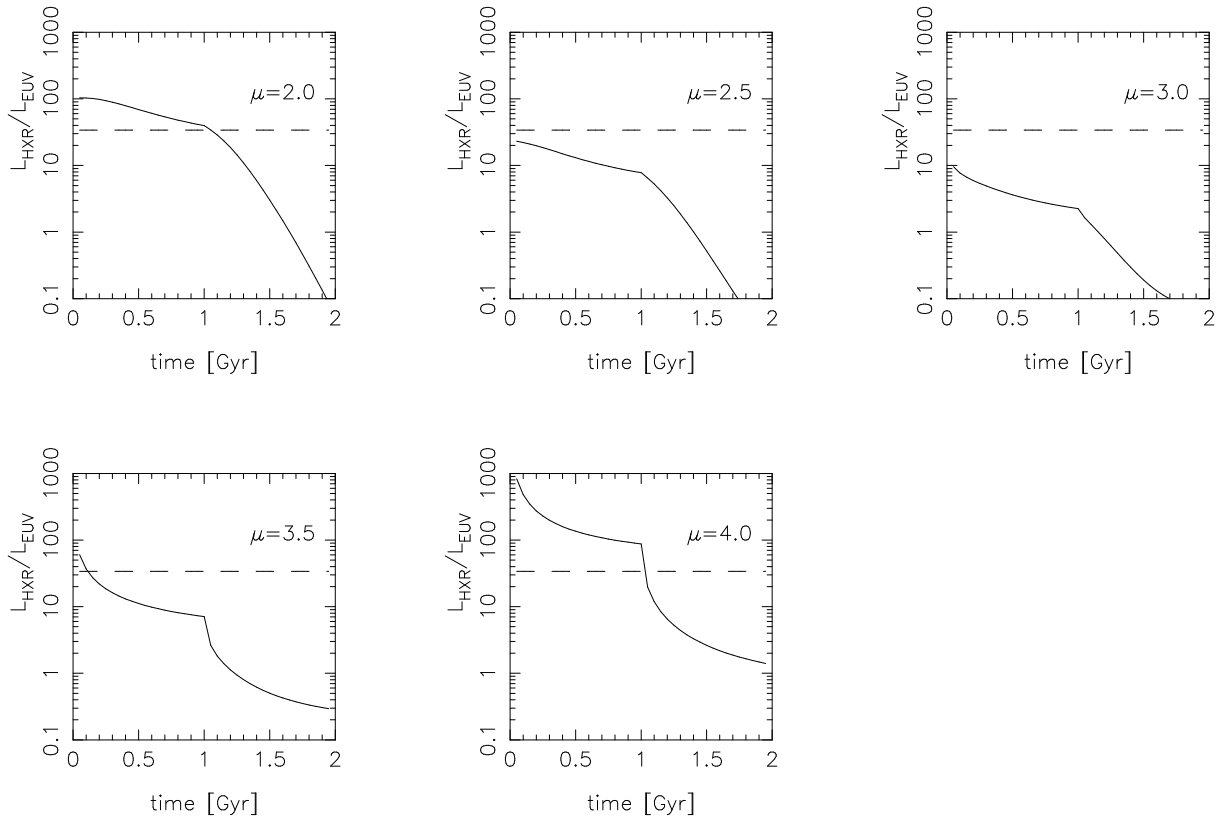


Fig. 6. Evolution of $L_{\text{HXR}}/L_{\text{EUV}}$ for each model (solid lines). Observed value of Coma derived from Fusco-Femiano et al. (1999) and Bowyer et al. (1999) is shown by dashed lines. Note that $L_{\text{HXR}}/L_{\text{EUV}}$ of our models must be more than the observed value. It is clear that this constraint is not satisfied when $\mu = 2.5$ and 3.0 . When $\mu = 3.5$, this can be satisfied only in a very early epoch ($t < 0.1$ Gyr). On the other hand, models with $\mu = 2.0$ and 4.0 satisfy the above-mentioned constraint in an active phase ($0 < t < 1$ Gyr).

of cluster magnetic field.

Our conclusions suggest that the momentum spectrum of the electron sources in Coma is fairly flat ($\mu < 2.5$). This is consistent with radio observations. Deiss et al. (1997) shows the radio spectral index in the frequencies lower than 1.4 GHz is -1.16 , which corresponds to $\mu = 2.32$ in the electron source term in a steady state (Note that equilibrium electron spectra are steeper than source spectra because of ICS cooling). However, this implies fairly high Mach number shocks. According to the standard theory of shock acceleration, $\mu < 2.5$ means a Mach number more than 3.0. This value is somewhat larger than estimated values (~ 2) of merger shocks from X-ray observations of other clusters (e.g., Markevitch, Sarazin, & Vikhlinin 1999; Kikuchi et al. 2000). However, estimated Mach numbers can be underestimated because observed temperature gradients can be underestimated owing to contamination by foreground and/or background ICM (Takizawa 2000, Shibata et al. 2001). Thus, it is possible that such 'hidden' high Mach number shocks contribute to particle acceleration in Coma. Indeed, merger shocks with a Mach number more than 3 do exist in numerical simulations of cosmological structure formation (Miniati et al. 2000). Another possibility is acceleration at external accretion shocks, which can be very high Mach number shocks because accreting gas is much colder than cluster virial temperature (Miniati et al. 2000).

Another possibility is reacceleration in intracluster space due to turbulent Alfvén waves and/or other physical process (Brunetti et al. 2001; Ohno, Takizawa, & Shibata 2001). In this case an electron spectrum can be much modified from an original source form. As a result, situation effectively similar to our $\mu = 2.0$ model possibly occurs though it depends on detailed acceleration history of non-thermal electrons.

In general, it is believed that non-thermal energy is less than thermal one in ICM. Only ICS dominant models with flat source spectra can satisfy this situation among our models. Even in this case, however, the obtained non-thermal to thermal energy ratio is fairly high. For example, TeV gamma-ray observation of SN1006 suggests this ratio is a few % (Tanimori et al. 1998), whereas our $\mu = 2.0$ model implies this ratio is more than 10 %. However, note that total energy of non-thermal electrons is sensitive to a spectral shape in lower energy. We assume that source spectra are power-law in momentum down to $E_e = 3kT$. This is valid when thermal electrons in ICM are the source of non-thermal electrons. However, this is not the case when old non-thermal electrons which leaked from AGNs and/or galaxies, and/or fossil radio plasma (Ensslin & Gopal-Krishna 2001) are the source. Once electrons are accelerated

Table 1. Comparison with the Coma cluster.

Model	$\log(\dot{E}_{\text{nth}})$ erg s ⁻¹	$\log(E_{\text{tot,nth}})$ erg	$\log(E_{\text{tot,nth}}/E_{\text{th}})$
$\mu = 2.0$	46.39	62.89	-0.77
2.5	47.51	64.01	0.35
3.0	49.13	65.63	1.97
3.5	49.87	66.37	2.71
4.0	50.08	66.58	2.93

up to ~ 100 MeV, they have a fairly long (\sim a few Gyr) life time. Thus, it is possible that lower boundary energy of single power-law is larger and that required energy is less.

I thank M. Henriksen and K. Nakazawa for fruitful discussion and S. Shibata for continuous encouragement. I would also like to thank the anonymous referee for very useful comments.

References

- Blasi, P. 2000, ApJ, 532, L9
Blasi, P., Olinto, A. V., & Stebbins, A. 2000, ApJ, 535, L71
Blumenthal, G., & Gould, R. 1970, Rev. Mod. Phys., 42, 237
Bowyer, S., Breghöfer, T. W., & Korpela, E. J. 1999, ApJ, 526, 592
Brunetti, G., Setti, G., Feretti, L., & Giovannini, G. 2001, MNRAS, 320, 365
Burns, J. O., Roettiger, K., Ledlow, M., & Klypin, A. 1994, ApJ, 427, L87
Cavaliere, A., & Fusco-Femiano, R. 1976, A&A, 49, 137
Clarke, T., Kronberg, P., & Böhringer H. 2001, ApJ, 547, L111
Deiss, B. M., Reich, W., Lesch, H., & Wielebinski, R. 1997, A&A, 321, 55
Dogiel, V. 2000, A&A, 357, 66
Ensslin, T., Lieu, R., & Biermann, P. 1999, A&A, 344, 409
Ensslin, T., & Kaiser, C. R. 2000, A&A, 360, 417
Ensslin, T., & Gopal-Krishna 2001, A&A, 366, 26
Fujita, Y., & Takahara, F. 1999a, ApJ, 519, L51
Fujita, Y., & Takahara, F. 1999b, ApJ, 519, L55
Fukazawa, Y., Nakazawa, K., Isobe, N., Makishima, K., Matsushita, K., Ohashi, T., & Kamae, T. 2001, ApJ, 546, L87
Fusco-Femiano, R., Fiume, D. D., Feretti, L., Giovannini, G., Grandi, P., Matt, G., Molendi, S., & Santangelo, A. 1999, ApJ, 513, L21
Fusco-Femiano, R., Fiume, D. D., De Grandi, S., Feretti, L., Giovannini, G., Grandi, P., Malizia, A., Matt, G., & Molendi, S. 2000, ApJ, 534, L7
Giovannini, G., Tordi, M., & Feretti, L. 1999, New Astronomy, 4, 141
Goldshmidt, O., & Rephaeli, Y. 1993, ApJ, 411, 518
Haug, E. 1997, A&A, 326, 417
Henriksen, M. 1999, ApJ, 511, 666
Inoue, S., & Sasaki, S. 2001, ApJ, 562, 618
Ishizaka, C., & Mineshige, S. 1996, PASJ 48, L37
Kaastra, J., Lieu, R., Mittaz, J., Bleeker, J., Mewe, R., Colafrancesco, S., & Lockman, F. 1999, ApJ, 519, L119
Kempner, J. C., & Sarazin, C. L. 2000, ApJ, 530, 282
Kikuchi, K. et al. 2000, ApJ, 531, L95
Kim, K.-T., Tribble, P. C., & Kronberg, P. P. 1991, ApJ, 379, 80
Koch, H. W., & Motz, J. W. 1959, Rev. Mod. Phys., 31, 920
Loeb, A., & Waxman, E. 2000, Nature, 405, 156
Longair, M. 1981, High Energy Astrophysics (Cambridge: Cambridge Univ. Press)
Markevitch, M., Sarazin, C. L., & Vikhlinin, A. 1999, ApJ, 521, 526
Miniati, F., Ryu, D., Kang, H., Jones, T. W., Cen, R., Ostriker, J. P. 2000, ApJ, 542, 608
Mohr, J. J., Mathiesen, B., & Evrard, A. E. 1999, ApJ, 517, 627
Ohno, H., Takizawa, M., & Shibata, S. 2001, ApJ, submitted
Petrosian, V. 2001, ApJ, 557, 560
Rephaeli, Y. 1979, ApJ, 227, 364
Rephaeli, Y., Ulmer, M., & Gruber, D. E. 1994, ApJ, 429, 554
Rephaeli, Y., & Silk, J. 1995, ApJ, 442, 91
Rephaeli, Y., Gruber, D., & Blanco, P. 1999, ApJ, 511, L21
Sarazin, C. L. 1999, ApJ, 520, 529
Sarazin, C. L., & Kempner, J. C. 2000, ApJ, 530, 282
Shibata, R. et al. 2001, ApJ, 549, 228
Takizawa, M. 1999, ApJ, 520, 514
Takizawa, M. 2000, ApJ, 532, 183
Takizawa, M., & Naito, T. 2000, ApJ, 535, 586
Tanimori, T. et al. 1998, ApJ, 497, L25
Totani, T. & Kitayama, T. 2000, ApJ, 545, 572
Valinia, A., Henriksen, M., Loewenstein, M., Roettiger, K., Mushotzky, R., & Madejski, G. 1999, ApJ, 515, 42
Watanabe, M., Yamashita, K., Furuzawa, A., Kunieda, H., Tawara, Y., & Honda, H. 1999, ApJ, 527, 80
Wilson, M. A. 1970, MNRAS, 151, 1